# EFFECT OF IN-PLANE CONSTRAINT AND TYPE OF LOADING ON FRACTURE TOUGHNESS OF TWO RPV STEELS OF PWRS

D. Lauerova, M. Brumovsky
Nuclear Research Institute Řež plc., 250 68 Řež, Czech Republic
lau@nri.cz, bru@nri.cz

## Abstract

In the frame of EU project VOCALIST, SE(B) and SE(T) specimens made of two reactor pressure vessel steels were tested and numerically evaluated at NRI Rez. The main aim of the VOCALIST project [1] was to quantify the constraint effect on fracture toughness for the steels mentioned, in particular, effect of shallow crack, loading mode and/or size effect on Master Curve reference temperature $T_0$. At NRI Rez, a total of 79 small fracture specimens were tested, the specimens contained either shallow or deep cracks, and both tension and bending types of loading were examined. For the individual groups of specimens (bending/tension specimens with deep/shallow cracks from material A/D) Master Curve reference temperatures $T_0$ were determined. For material D, smaller values of $T_0$ for tension than for bending were found, both for deep and shallow cracks. *J-Q* loci for materials A and D for selected temperatures were constructed. For the purpose of engineering assessment, using of lower bound curves of the *J-Q* locus for conservative fracture prediction is suggested.

## Introduction

The VOCALIST project was focused on examination of constraint effects on fracture toughness; these effects were examined primarily on two reactor pressure vessel steels (materials A and D) and also on one ferritic piping steel (material P) [1]. At NRI Rez, only specimens from materials A and D were tested. Material A was a forged, quenched and tempered ring segment of the ferritic steel DIN 22 NiMoCr 3 7, which corresponds to ASTM A508 Grade 3 Class 1, with properties representative of an RPV at start of life. Material D is a A533B ferritic steel plate heat treated to achieve an elevated yield strength representative of an RPV that has undergone in-service exposure to neutron irradiation.

Within the VOCALIST Project mainly effects of crack depth, specimen size and type of loading were examined. At NRI Rez, fracture toughness tests on small specimens from materials A and D were performed with the main goal to determine the Master Curve (MC) reference temperature $T_0$ as well as shift in this temperature, $\Delta T_0$, due to shallow crack effect. For material D, both bending and tension specimens were tested, while for material A only tension specimens were tested.

In what follows, FE evaluation of the tests is described, encompassing primarily determination of fracture toughness values ($J_c$) for all tested specimens, and for selected groups of specimens also determination of *Q*-stress parameter values. The determined fracture values of *J* and *Q* were used to construct *J-Q* loci for both materials A and D.

## Evaluation of tests performed on specimens from material D

For material D, both bending SE(B) and tension SE(T) specimens were tested. Geometry of bending specimens was as follows: Pre-cracked Charpy, with net test section 10 x 8 mm, with side grooving. Specimens were subject to 3 point bending. 16 specimens with deep cracks ($a/W$~0.5) and 16 specimens with shallow cracks ($a/W$~0.1) were tested.

Geometry of tension specimens is seen in Fig. 1. 12 SE(T) specimens containing deep cracks and 12 SE(T) specimens containing shallow cracks were tested. Tension specimens also contained side grooves. Average values of crack depths for all specimens are summarized in Table 1.

Specimens were tested at the following test temperatures: Bending specimens with deep cracks at –60 ºC, –80 ºC and –90 ºC, bending specimens with shallow cracks at -80 ºC, –90 ºC and –110 ºC, tension specimens with deep cracks at –60 ºC, –80 ºC and –90 ºC, tension specimens with shallow cracks at –80 ºC, –90 ºC and –110 ºC.

In FE calculations, material elastic properties were described using values of Young modulus and Poisson ratio $E$ = 210 GPa and $\nu$ = 0.3, respectively. Plastic properties were introduced using stress-strain curves plotted in Fig. 2. Details of yield strengths, ultimate strengths, uniform elongations and proportionality limits for material D may be found in [2].

In the tests, values of force and CMOD (crack mouth opening displacement) were recorded. All specimens failed by cleavage. Some of the bending specimens experienced small amount of ductile tearing before cleavage fracture, not higher than 0.2 mm (individual value over crack front). For tension specimens, no ductile tearing prior to cleavage was observed.

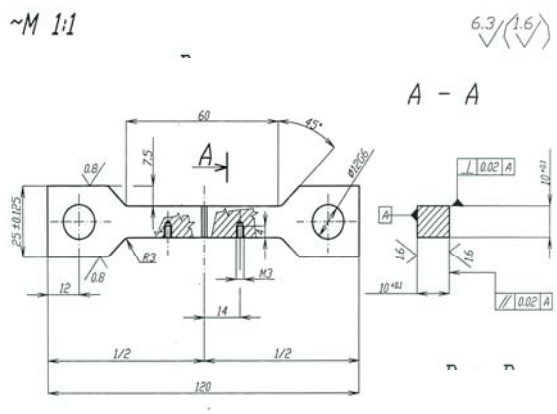


FIGURE 1. Scheme of tension specimen, materials A and D

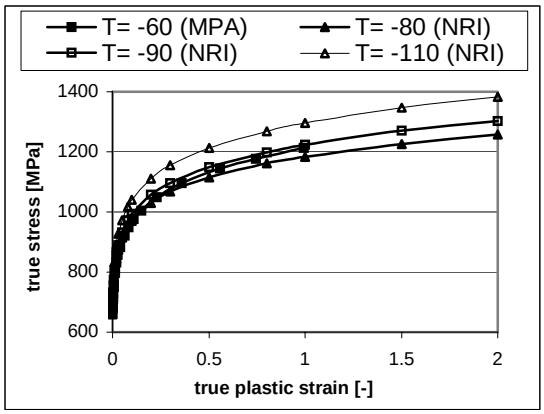


FIGURE 2. Stress-strain curves used in FE calculations for material D

### *Numerical analysis of experimental data*

FE calculations were performed using FE code SYSTUS. 3D quadratic meshes were constructed for all specimens. Due to symmetry of specimens, only ¼ of the specimen was modeled. Mesh near crack front was of radial type (pentahedrons), with element size near crack front of 0.01 mm. Crack front was modeled straight, with crack depth equal

approximately to the average crack depth; usually one FE calculation was used for evaluation of several specimens having approximately the same crack depth.

Elastic-plastic behavior of specimens was modeled using flow theory of plasticity with von Mises yield surface and isotropic strain hardening. Large strains (updated Lagrangian formulation) were used.

For evaluation of *J*-integrals, SYSTUS fracture mechanics module based on G-theta field was used.

### *Evaluation of bending specimens*

Due to lack of space, neither experimental nor computed force vs. CMOD curves are presented in the paper. In most cases, the accordance between experimental and computed curves was good - details may be seen in [2].

Values of fracture toughness $J_c$ for bending specimens were evaluated both experimentally and numerically using FE calculations. Experimental values $J_c$ were determined using $\eta_{pl}$ factors [3]. Comparison between experimental and FE based values $J_c$ may be seen in Figs. 3 and 4. It is seen from Fig. 3, that for deep cracks FE values $J_c$ are systematically a little higher than the experimental ones. The difference is small and may be a consequence of selection of input parameters for the *G*-theta module used in FE evaluation of *J*-integrals. For shallow cracks (Fig. 4), no systematic deviation from the 1:1 line is observed, but with increasing loading the experimental values of fracture toughness become higher than the FE ones.

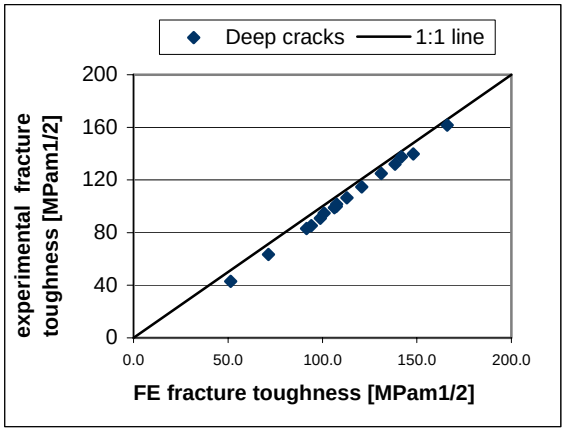


FIGURE 3. Experimental vs. FE values of $J_c$, bending specimens, deep cracks

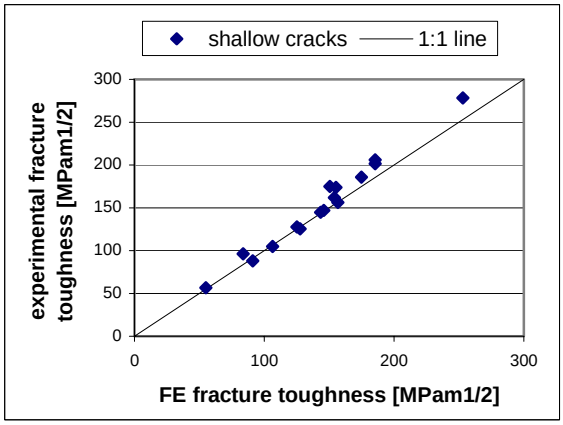


FIGURE 4. Experimental vs. FE values of $J_c$, bending specimens, shallow cracks

After adjustment to 1T thickness, the experimental fracture toughness values of bending specimens are seen in Fig. 5. Master Curve reference temperatures were determined using multi-temperature approach [4], for deep and shallow cracks and for both experimental and FE values of $K_{Jc}$. The respective $T_0$ values are seen, together with values of $T_0$ resulting from tension specimens, in the Table 1. The shift in $T_0$ due to shallow crack effect (loss of in-plane constraint) for bending specimens, material D, is presented in Table 2, together with shifts in $T_0$ for tension specimens of materials A and D.

## *Evaluation of tension specimens*

Fracture toughness values $J_c$ for tension specimens were determined based on FE calculations, since for this type of specimen no fully verified force vs. CMOD based formulae for determination of $J_c$ are available. For determination of $J_c$, the same values of input parameters for the *G*-theta module as with bending specimens were used. FE values of $J_c$ were expressed in terms of $K_{Jc}$-values and, after adjusting to 1T thickness, they are seen in Fig. 6.

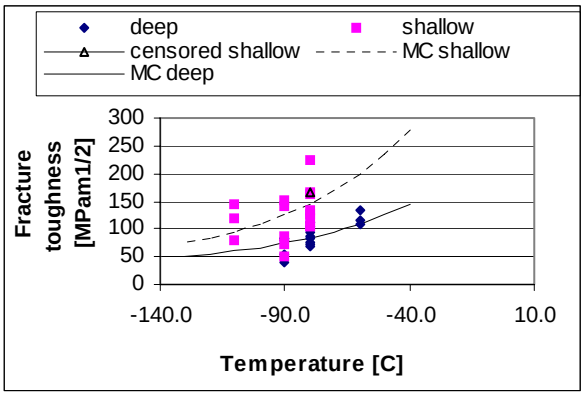


FIGURE 5. Experimental values of $J_c$ adjusted to 1T, bending specimens, material D

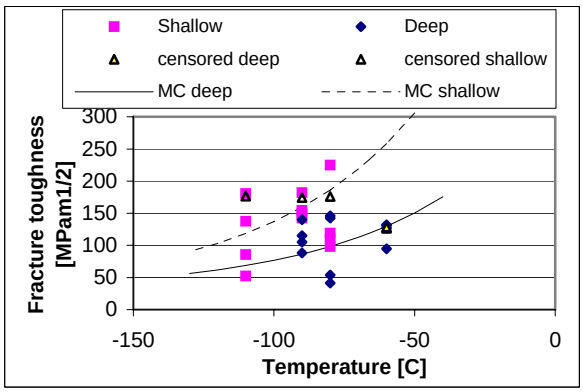


FIGURE 6. FE based values of $J_c$ adjusted to 1T, tension specimens, material D

### *Construction of Q-fields and J-Q loci for material D*

For selected temperatures, –80 ºC and -90 ºC, the *Q*-stress values at fracture were determined for both bending and tension specimens of material D. *Q*-stress fields as functions of normalized distance $r\sigma_0/J$ were calculated using the formula

$$Q = \frac{\sigma_{yy} - (\sigma_{yy})_{\mathrm{SSY},T=0}}{\sigma_0},$$

where $\sigma_{yy}$ is the stress opening the crack for the examined specimen (full model), $(\sigma_{yy})_{\mathrm{SSY},\,T=0}$ is stress opening the crack for reference SSY (small scale yielding) solution with *T*-stress = 0, $\sigma_0$ is the yield stress. Values of $\sigma_{yy}$ and $(\sigma_{yy})_{\mathrm{SSY},\,T=0}$ were determined always on symmetry plane ($\theta$=0). Reference solution $(\sigma_{yy})_{\mathrm{SSY},\,T=0}$ was obtained by solving the Modified Boundary Layer Problem in 2D (plane strain). *Q*-stress fields were calculated always for fracture load.

The resulting *Q*-fields as functions of normalized distance $r\sigma_0/J$ for individual bending and tension specimens at fracture load are seen in Figs. 7 and 8, respectively. From these figures several conclusions may be drawn that are applicable both for bending and tension specimens:

1) specimens with shallow cracks exhibit significant loss of constraint compared to specimens with deep cracks, in consequence of which *Q*-fields for shallow cracks lie significantly lower than those for deep cracks
2) Within each of the four examined groups of specimens (bending/tension specimens with deep/shallow cracks), basic trend may be seen: *Q*-fields are decreasing with increasing *J* and decreasing *a/W* (*W* being constant)
3) *Q*-fields for deep cracks, with the exceptions of those corresponding to specimens that failed at very low load, "drop" within interval (2,10), having no region of "flat minimum" within this interval

4) $Q$-fields for shallow cracks exhibit some region of "flat minimum" within interval (2,10), with the exception of tension specimen TSFC3 (Fig. 9) that experienced the highest loading. The $Q$-field for this specimen has also a minimum (though not flat) that lies in the vicinity of $r\sigma_0/J = 1.9$, in consequence of which it is not seen in Fig. 9.

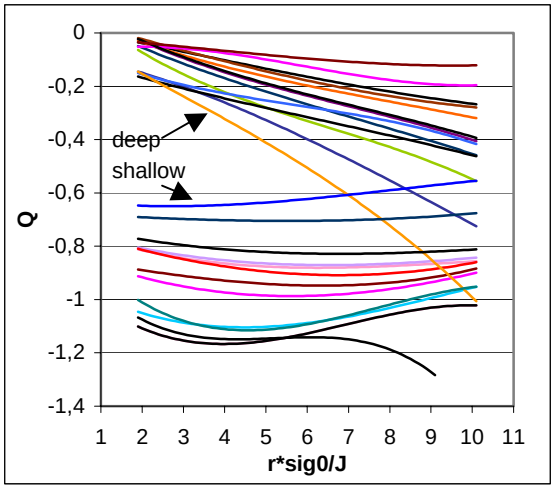


FIGURE 7. $Q$-fields for bend specimens, $T$= -80 ºC and –90 ºC

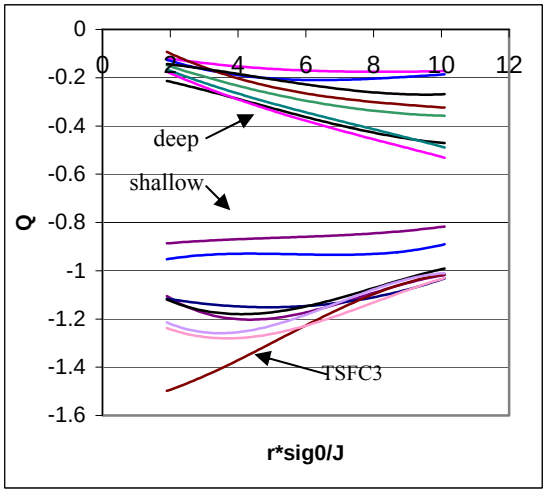


FIGURE 8. $Q$-fields for tension specimens, $T$= -80 ºC and –90 ºC

Variations of $Q$-fields within interval (2,10) have, of course, consequences for construction of the $J$-$Q$ locus. In association with this, a question arises: in which point of interval (2,10) the $Q$-stress parameter should be determined? This problem was in more details examined in [7] using statistical treatment, but no definite conclusion was drawn in [7], since this problem is of complex character. Its solution depends, among others, on which requirements Q should meet. The requirements posed on $Q$ may be as follows: (1) $Q$ should equal $T$ in the region of elasticity and lower levels of plasticity, (2) $Q$ should be an interval-wide value, not a point-measure [6], (3) $Q$ should scale with loading (for constant crack depth). Globally, it may be said that it is not easy to fulfill all these requirements simultaneously. In our case (Figs. 7 and 8) $Q$-fields for tension specimens with shallow cracks fulfil requirement (3) in some subinterval containing the point $r\sigma_0/J = 2$, but this is not the case for $Q$-fields of bend specimens with deep cracks (they do not scale with loading in the vicinity of the point $r\sigma_0/J = 2$). Further, $Q$-fields for specimens with deep cracks for either tension or bending do not fulfil requirement (2) in any subinterval of interval (2,10). Taking into account all these facts, we may conclude that for the purpose of transferability of fracture parameters between different geometries and configurations, it should be always mentioned in which point $Q$ was determined and also, the shapes of $Q$-fields should be shown, if possible.

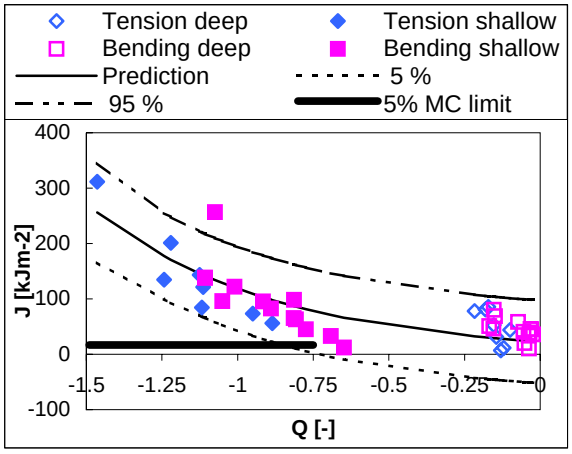


FIGURE 9. *J-Q* locus for material D. The *Q*-parameter is determined at $r\sigma_0/J$=2.

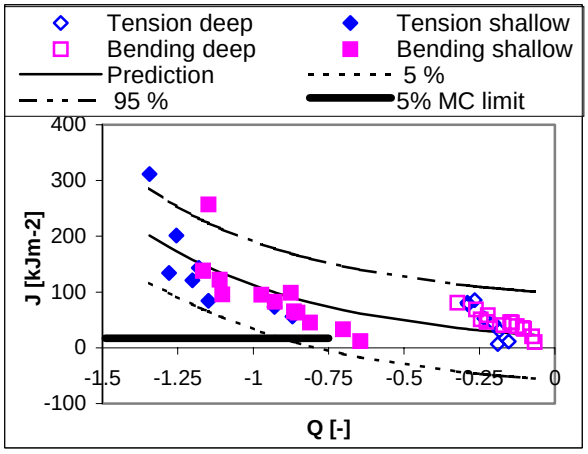


FIGURE 10. *J-Q* locus for material D. The *Q*-parameter is determined at $r\sigma_0/J$=4.

In the present paper, the *J-Q* loci for material D are constructed for *Q* determined in $r\sigma_0/J$ = 2 and 4. These *J-Q* loci are seen in Figs. 9 – 10, together with the "Prediction" curve that represents dependence of type $y=a*\exp(-bx)$ with parameters $a,b>0$ found by nonlinear regression, the appropriate 5% lower and upper bound curves (predictions for individual value) determined also by nonlinear regression, and 5% Master Curve limit. Since the *Q*-parameter depends on loading and due to statistical character of cleavage fracture, the *J-Q* locus as such (or some kind of "median curve" of *J-Q* locus) is not suitable for prediction of fracture. But for the lower bound curve of *J-Q* locus, this argument is no more valid, in other words, lower bound curve is in fact independent of loading and may be, at least in principle, used for conservative prediction of fracture in engineering assessment. It is seen from Figs. 9 and 10 that some benefit from considering the constraint effect (via the *J-Q* locus) may be obtained for $Q < -0.9$ approximately, since for these values of *Q* the 5% lower bound curve rises above the 5% MC limit usually used in reactor pressure vessel integrity evaluation based on Master Curve approach.

## Evaluation of tests performed on specimens from material A

For material A, only tension specimens SE(T) with deep and shallow cracks were tested at NRI Rez. Geometry of tension specimens was the same as for material D (Fig. 1).

Specimens with deep cracks were tested at temperatures –100 ºC, –120 ºC, and –130 ºC. Specimens with shallow cracks were tested at temperatures –120 ºC, –130 ºC, and –150 ºC. Average crack depths for deep/shallow cracks are attached in Table 1.

In FE calculations stress-strain curves obtained from Framatome ANP GmbH were used. Due to lack of space, we do not attach these curves here, they may be found e.g. in [2].

During experiments, values of force and CMOD were recorded. All specimens failed by cleavage, no crack extension due to ductile tearing was observed.

## FE Analysis - Determination of $J_c$ and $K_{Jc}$ values

As in case of material D, $J_c$-values for tension specimens of material A were determined using $G$-theta module of FE code SYSTUS. Within this procedure, the same values of input parameters of the G-theta module were used as for material D.

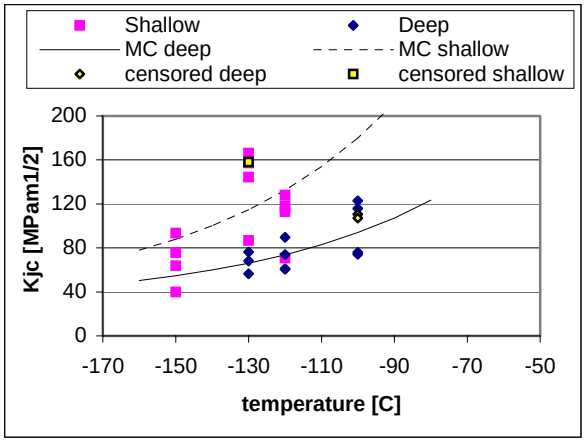


FIGURE 11. FE values of $J_c$ adjusted to 1T, for tension specimens of material A

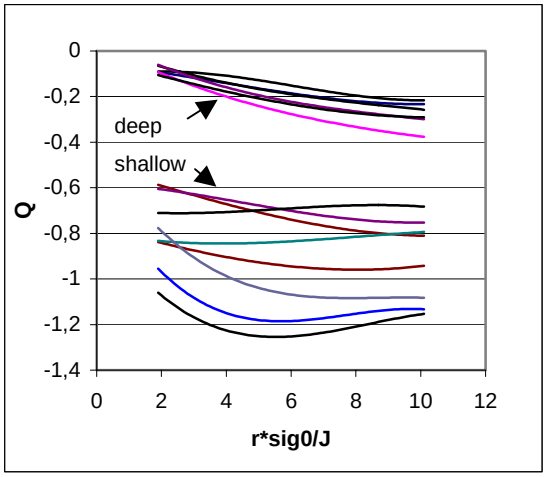


FIGURE 12. $Q$-fields for tension specimens of material A, $T$= -120 ºC and -130 ºC

After converting the $J_c$-values into the $K_{Jc}$-values and adjusting to 1T thickness, they are seen in Fig. 11, together with the appropriate Master Curves.

Multi-temperature approach was used to determine Master Curve reference temperatures $T_0$ for deep and shallow cracks. The appropriate $T_0$ values are seen in the Table 1. The shift in $T_0$ due to the shallow crack effect for these specimens is presented in Table 2.

### *Construction of Q-fields and J-Q loci for material A*

$Q$-fields for tension specimens from material A (at fracture) were determined for temperatures -120 ºC and -130 ºC, using the same approach as in the case of material D. The $Q$-fields are seen in Fig. 12.

The appropriate $J$-$Q$ loci (fracture values), both for case of $Q$ determined in $r\sigma_0/J$=2 and in $r\sigma_0/J$=8 are seen in Figs. 13-14. From these figures it is seen that determination of $Q$-parameter at the point $r\sigma_0/J$=8 decreases the relative scatter significantly compared to case when $Q$ is determined at $r\sigma_0/J$=2. Nevertheless, in both cases the 5% lower bound curve of the $J$-$Q$ locus rises above the 5% MC limit (usually used in integrity evaluation) for $Q$ < -0.8 approximately, and for these $Q$-values some benefit of constraint effect within $J$-$Q$ approach may be obtained.

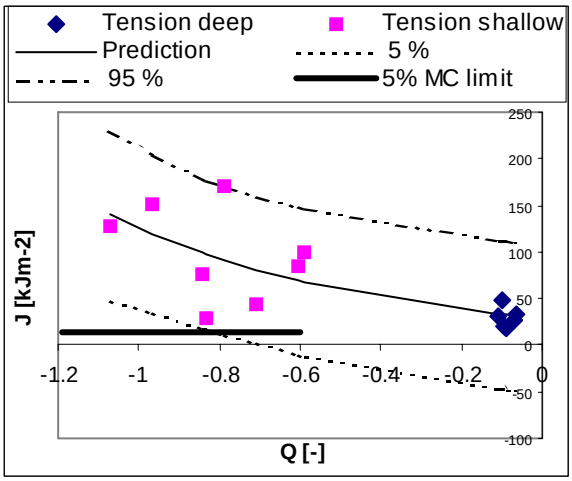


FIGURE 13. *J-Q* locus for material A. *Q* determined at $r\sigma_0/J$=2

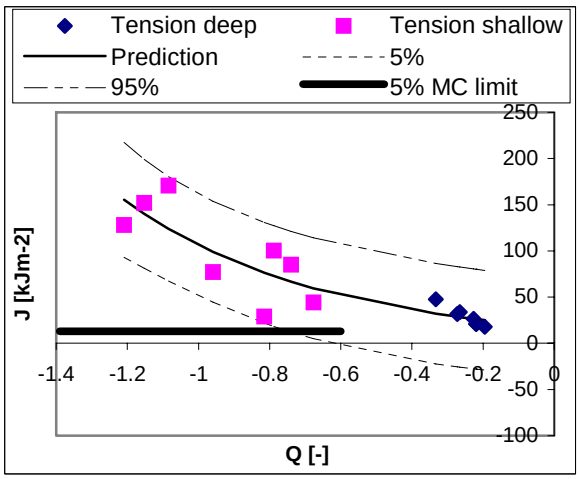


FIGURE 14. *J-Q* locus for material A. Q determined at $r\sigma_0/J$=8

## Discussion of shallow crack effect and effect of type of loading on $T_0$

Shifts in $T_0$ due to shallow crack effect were calculated from values of $T_0$ presented in Table 1 for both materials A and D. The results are summarized in Table 2. As seen from Table 2, practically the same shift ($\Delta T_0 \approx 44$ ºC) was found for tension specimens of material A and tension specimens of material D. For bending specimens (material D), the effect of shallow crack was a little less pronounced than for tension specimens, mainly when comparing FE values of the shifts ($\Delta T_0 \approx 31.6$ ºC).

When examining the effect of loading configuration on $T_0$, it may be seen from Table 1 that for material D values of $T_0$ for tension are lower than those for bending, both for deep and shallow cracks; the difference is 8.5 ºC for deep cracks, and 20.6 ºC for shallow cracks. This result suggests that tension type of loading alone may result in loss of constraint.

## Conclusions

Evaluating separately the specimens tested at NRI, effect of shallow crack was clearly proved and quantified in terms of $T_0$ shift. Approximately the same shifts were found for tension specimens of material D and those of material A (≈ 44 ºC). For bend specimens of material D, the $T_0$-shift due to shallow crack effect was found a little lower (32 ÷ 41 ºC).

Effect of type of loading (comparing SE(B) specimens with SE(T) ones) was found for material D: Values of $T_0$ for tension specimens (both for deep and shallow cracks) were lower (8.5 ºC, 20.6 ºC) than those for bending specimens.

*J-Q* loci for materials A and D were constructed, the shapes of *J-Q* locus being moderately dependent on value of normalized distance where the *Q*-parameter is determined. For the purpose of engineering assessment, 5% lower bound curves of the *J-Q* loci were constructed and the possible benefit of using them in integrity evaluation based on Master Curve approach was shown.

**Table 1**. **MC reference temperatures $T_0$ for materials D and A**

| Material | Type of loading | Type of crack | Average $a/W$ | Experimental/calculated fracture toughness | $T_0$ [C] |
|---|---|---|---|---|---|
| D | Bending | Deep | 0.46 | Calculated | -70.0 |
| D | Bending | Deep | | Experimental | -66.0 |
| D | Bending | Shallow | 0.11 | Calculated | -101.6 |
| D | Bending | Shallow | | Experimental | -106.5 |
| D | Tension | Deep | 0.52 | Calculated | -78.5 |
| D | Tension | Shallow | 0.13 | Calculated | -122.2 |
| A | Tension | Deep | 0.56 | Calculated | -95.2 |
| A | Tension | Shallow | 0.17 | Calculated | -140.1 |

**Table 2**. **Shifts in $T_0$ due to shallow crack effect found for materials A and D**

| Type of loading | Shift in $T_0$ [ºC] | |
|---|---|---|
| | Material D (Experimental/FE value) | Material A |
| Bending | 40.5 (exper.) / 31.6 (FE) | - |
| Tension | 43.7 (FE) | 44.9 (FE) |

## REFERENCES


1. Lidbury, D. et al.: Validation of Constrained Based Methodology in Structural Integrity (VOCALIST). *FISA-2003, EU Research in Reactor Safety*, 10-13 November, EC Luxembourg
2. Lauerova, D. et al.: *Evaluation of Characterization Tests performed on Tension and Bending Specimens for Material A and D*. Report NRI Rez, DITE 301/265/R1, January 2004.
3. VOCALIST WP 3: J-evaluation from SE(B)- /SE(T)-tests. WP3 – Testing Recommendations. Distributed to VOCALIST WP3-partners by U. Eisele, MPA Stuttgart.
4. ASTM Standard E 1921 – 02. Standard Test Method for Determination of Reference Temperature, $T_0$, for Ferritic Steels in the Transition Range, June 2002.
5. Lauerova, D., Brumovsky M.: In *Proceedings of the ASME PVP Conference*, San Diego, 2004, to appear.
6. Faleskog, J.: Effects of Local Constraint along Three-dimensional Crack Fronts – a Numerical and Experimental Investigation, in *J.Mech. Phys. Solids*, Vol. 43, No. 3, pp. 447 – 493, 1995.